Journal of Applied Polymer Science

Polylactide/Halloysite Nanotube Nanocomposites: Thermal, Mechanical Properties, and Foam Processing

Wei Wu, Xianwu Cao, Yijun Zhang, Guangjian He

National Engineering Research Center of Novel Equipment for Polymer Processing, National Engineering Laboratory for Plastic Modification and Processing, Key Laboratory of Polymer Processing Engineering of Ministry of Education, School of Mechanical and Automotive Engineering, South China University of Technology, Guangzhou 510640, People's Republic of China

Correspondence to: X. Cao (E-mail: ppeme@scut.edu.cn)

ABSTRACT: Polylactide (PLA)/halloysite nanotube (HNT) nanocomposites with different HNT contents were prepared by melt compounding. The morphology, crystallization behavior, as well as thermal and mechanical properties of the nanocomposites were studied. The results showed that HNT were well dispersed in PLA matrix. Thermogravimetric analysis data revealed that the thermal stability of PLA was decreased with the increasing of HNT content. Differential scanning calorimetry analysis indicated that the presence of HNT could promote cold crystallization and lead to different crystalline phase formation. The flexural and tensile modulus of PLA/HNT nanocomposites improved significantly with the incorporation of HNT. Compared with neat PLA foam, PLA/HNT nanocomposite foams showed much higher cell density and smaller cell size due to HNT serving as the heterogeneous nucleating agents.
 J. Appl. Polym. Sci. 130: 443–452, 2013

KEYWORDS: polyesters; composites; foams; mechanical properties

Received 24 November 2012; accepted 16 February 2013; published online 18 March 2013
DOI: 10.1002/app.39179

INTRODUCTION

Bio-based polylactide (PLA), generally chemically synthesized polycondensation by lactide, is a thermoplastic aliphatic polyester with many attractive properties, including biodegradability and biocompatibility. It is a well-known biodegradable material that living organisms can degrade them rapidly into carbon dioxide, water, and humus under appropriate conditions.[1] The environment-friendly polyester can replace commodity polymers in various applications, such as drug delivery, tissue engineering, and packaging industries. However, PLA needs to be modified for enhanced some of its properties such as poor melt strength, low heat deflection temperature, and slow crystallization kinetics in some applications. To improve these performances, copolymerization, melt blending, and particle compounding have been explored.[2–6] The incorporation of clay into the PLA matrix has attracted much attention in both the academic and industrial fields due to their enhanced physical and mechanical properties compared with pure PLA.[7–13] The PLA/clay nanocomposites can be mainly prepared by three different methods: *in situ* polymerization,[14,15] solution intercalation,[16,17] and melt blending.[7,9,18] The melt blending method stands out among the methods for industrial applications due to no use of organic solvent, highly efficient and compatible with current industrial processing techniques.

Polymer foams have been widely used because of their low density, poor thermal and sound conductivity, and excellent strength-to-weight ratio characteristics.[19] A wealth of papers dealing with PLA/clay nanocomposite foams has been reported. Okamoto and coworkers[20] had pioneered to prepare PLA nanocomposite foams in a batch process by using supercritical carbon dioxide (Sc-CO_2) as a physical foaming agent. The morphology observation showed that the cell nucleation took place at the boundary between PLA matrix and clay particles, and the addition of clays could help to control the foam structure. Di et al.[21] found that the existence of a low amount of organic clay into the foam formulation was an effective way to modify the processing behavior of the polymeric matrix. The PLA nanocomposite foams showed the smaller cell size and higher cell density in comparison with neat PLA foam. Similar results also have been reported by other researchers.[22–24] Matuana and Diaz[25] found that the presence of nano-clay could increase the heterogeneous nucleation, allowing both homogeneously and heterogeneously nucleated cells grow simultaneously during extrusion foaming processing.

Halloysite nanotubes (HNT) are generally known as a type of natural silicate nanotubes, which have the same chemical composition as kaolinite.[26] Similar to multiwall carbon nanotubes, HNT exhibit a hollow tubular structure as the dominant

morphology. The outer diameter of HNT ranged from 10 to 50 nm, the inner diameter ranged from 5 to 20 nm with typical 2–40 μm in length.[27] Owing to the multilayer crystal structure, special hollow structure, and low density of hydroxyl functional groups on the surface, they are relatively easy to get a good dispersion in the polymer matrix compared with other nanoclays.[28] Thus, they have been used as novel filler to fabricate polymer/HNT nanocomposites.[29–33] Tang et al.[30] found that the addition of HNT could increase the fracture toughness of epoxy composites without sacrificing strength, modulus, and thermal stability. Ning et al.[33] investigated the effect of HNT on the crystallization rate of polypropylene and found HNT could act as a nucleation agent to promote the overall crystallization rate of polypropylene. Jia et al.[34] showed that HNT could enhance mechanical properties and improve the flame retardant of linear low density polyethylene. But the application of HNT in polymer foams has not been reported.

The purpose of this article is to fabricate the PLA/HNT nanocomposite and process the nanocomposite foam by using Sc-CO_2. The morphology, thermal, and mechanical properties of the PLA/HNT nanocomposites are characterized before producing the foams.

EXPERIMENTAL

Materials

A commercially available PLA (grade 2002D) was purchased from NatureWorks. The HNT (grade ultrafine) was supplied by Imerys Tableware Asia Limited, Auckland, New Zealand. The density of neat HNT is ~2.55 g/cm^3. The carbon dioxide (CO_2) with a purity of 99.9% obtained from Golden Zhujiang Chemical Co., Guangzhou, China, was used as the physical blowing agent. All the materials were used as received.

Preparation of PLA/HNT Nanocomposites

Before sample preparation, PLA pellets and HNT were dried in a vacuum oven for 8 h at 80°C and 95°C, respectively. PLA/HNT nanocomposites with different weight ratios (99/1, 97/3, 95/5, and 93/7 w/w) were prepared by melt compounding using a counter-rotating internal mixer (PLASTIC-ORDER, Brabender, Germany) with a rotation speed of 60 rpm for 5 min at 180°C. The obtained PLA/HNT nanocomposites were named as PLA1, PLA3, PLA5, and PLA7, respectively. Pure PLA was named sample PLA0. The neat PLA and PLA/HNT nanocomposites were subsequently molded into specimens by using compression molding (180°C, 10 min) to measure their properties and prepare for foams.

Foam Processing

Neat PLA and PLA/HNT nanocomposites foams were prepared via a batch processing method by using Sc-CO_2 as physical blowing agent. The schematic diagram of foam processing is shown in Figure 1. Briefly, the sample is put into a cupboard-shaped mold and load in an autoclave. The autoclave will be preheated to a certain temperature, 105°C, 115°C, 125°C, and 135°C, respectively. Then, CO_2 is delivered into the autoclave till the pressure in the autoclave rise to 20 MPa with a positive-displacement syringe pumps (model 260D; Teledyne Isco). After the sample immersing in CO_2 for 2 h under 20 MPa pressure at desired temperature, foam expansion is induced by the sudden gas release and the gas rapid depressurization is less than 5 s. The formed foam samples are stabilized via rapidly cooling to room temperature and then remove carefully from the mold.

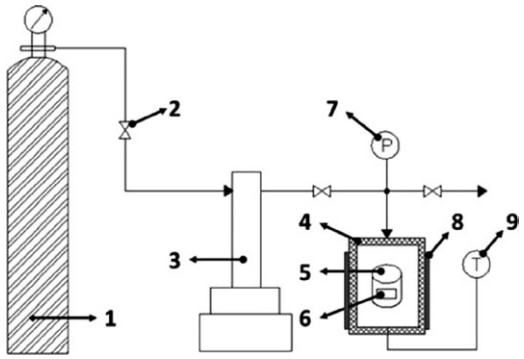

Figure 1. Schematic diagram of a custom-designed high pressure supercritical CO_2 foaming instrument: (1) CO_2 gas cylinder, (2) valve, (3) syringe pumps, (4) autoclave, (5) mold, (6) sample, (7) pressure gauge, (8) heater, and (9) temperature controller.

Thermogravimetric Analysis

Thermal stability of HNT and PLA/HNT nanocomposite was measured using a thermogravimetric analyzer (TG209, Netzch, Germany), by heating from 30°C to 700°C at the heating rate of 10°C/min under nitrogen atmosphere.

Differential Scanning Calorimetry

The crystallization behavior of the nanocomposite was also studied by using the differential scanning calorimetry (DSC 8000, PerkinElmer). Samples about 5 mg were heated from room temperature to 200°C with a heating rate of 10°C/min and the temperature was held at 200°C for 3 min to eliminate the previous thermal history. Then, the melted samples were cooled to 20°C with the cooling rate of 10°C/min and again heated to 200°C at the predetermined rate subsequently. The exothermic and second endothermic curves of heat flow as a function of temperature were recorded to analyze the nonisothermal crystallization process of the nanocomposite. All the experiments were performed under nitrogen atmosphere.

Mechanical Testing

Tensile and flexural properties of the nanocomposite samples were determined by an electronic universal testing machine (model 5566, Instron) with a 10 kN load cell. The tensile specimens (dumbbell-shaped) with testing area: 25 mm × 4 mm × 1 mm were tested at a crosshead speed of 1 mm/min according to GB/T 16421-1996. Flexural modulus and strength of the specimens (thickness about 4 mm) were measured in accordance with GB/T 9341-2000 with a strain rate of 1 mm/min. The reported data were the average of five successful tests.

Scanning Electron Microscopy

The distribution of HNT in the PLA matrix was observed via Scanning Electron Microscopy (SEM) (Nano 430, FEI). The cell morphologies of fractured foam specimens were also elucidated. Before SEM observation, the specimens of PLA/HNT nanocomposites were frozen fractured in liquid nitrogen for around 10 min and then all specimens were sputtered with gold.

To quantitatively assess the SEM micrographs with respect to the cell structures, Image-Pro Plus software (Beta 4.0, Media Cybernetics Corp.) was used to convert the SEM gray-level image into a binary image by setting an appropriate brightness threshold. Through the analysis of the SEM photomicrographs of foamed samples, the cell density (ρ_c) could be calculated using the following equation[35]:

$$\rho_c = \left(\frac{NM^2}{A}\right)^{3/2} \quad (1)$$

where A is the area of the SEM micrograph, N is the number of cells in the area A, and M is the magnification factor of the SEM micrograph. To evaluate the mean cell diameter and cell density, about 100 cells in the SEM micrographs of each sample were calculated.

RESULTS AND DISCUSSION

Morphology of Fractured Samples

SEM observation was conducted on fractured samples to investigate the HNT dispersion in the nanocomposite. It is one of the most important factors for improving the mechanical, electrical, and thermal performances of a polymer matrix. Figure 2 shows typical SEM micrographs of the fractured surface of PLA/HNT nanocomposite. It can be seen that most of the HNT are dispersed uniformly in PLA matrix, and only a few aggregates are found in the PLA/HNT nanocomposite. The good dispersion of HNTs in the other polymers was also reported.[36,37] Furthermore, the micrographs also indicate that some HNT is exposed on the surface and a great deal of cavities can be seen, suggesting a poor interaction between the surface of the NHT and the PLA matrix.

Thermal Stability

The dried HNT was tested by the thermogravimetric analysis (TGA) (Figure 3). As reported in the literature,[34] the main mass loss of neat HNT about 11% at the temperature range of 400°C–550°C is attributed to the release of the crystal water.

The TGA and DTG thermograms for the PLA/HNT nanocomposite in nitrogen are shown in Figure 4. The decomposition temperatures (5% and 10% weight loss) are summarized in Table I. It is usually believed that the thermal barrier and the mass transport barrier properties of nano-filler will enhance thermal stability of the polymer matrix.[38] However, the data reveals that the temperatures at 5% weight loss of PLA/HNT

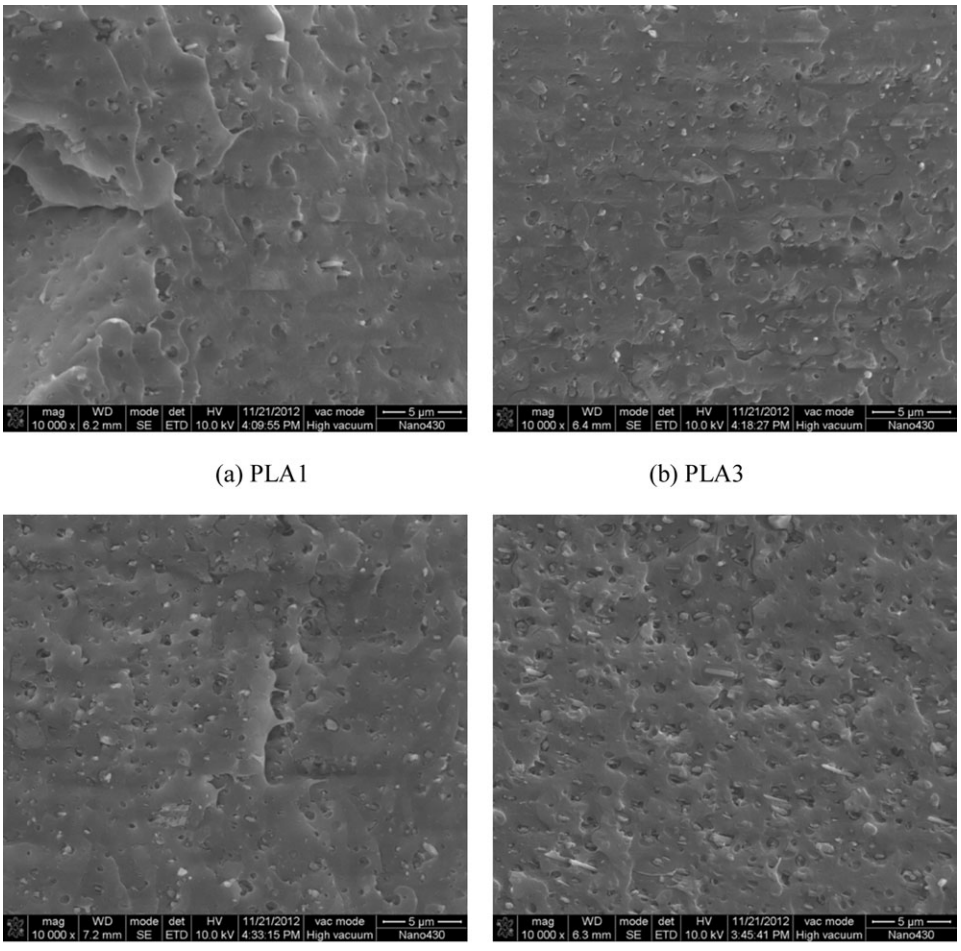

Figure 2. SEM images of the PLA/HNT nanocomposite: (a) PLA1, (b) PLA3, (c) PLA5, and (d) PLA7.

Applied Polymer SCIENCE

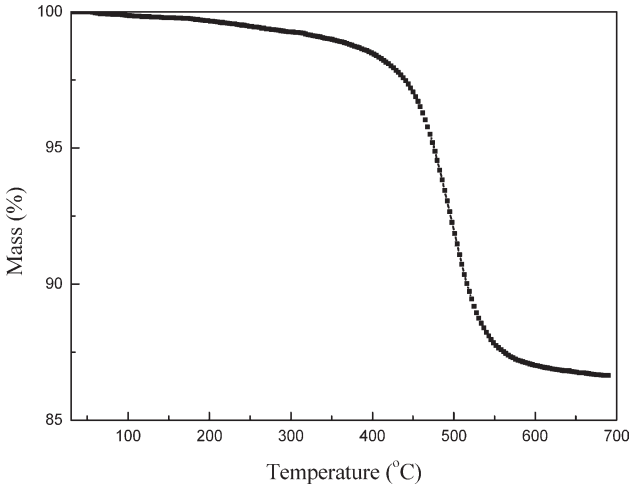

Figure 3. TGA thermograms of HNT.

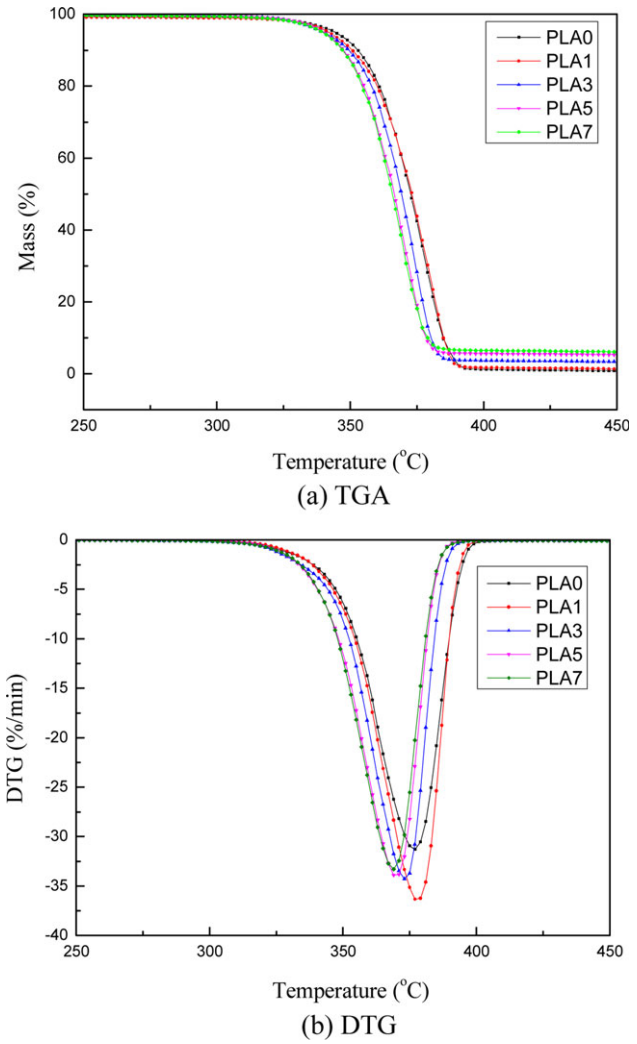

Figure 4. TGA thermograms of neat PLA and PLA/HNT nanocomposites (a) TGA and (b) DTG. [Color figure can be viewed in the online issue, which is available at wileyonlinelibrary.com.]

Table I. TGA Data of PLA/HNT Nanocomposites in Nitrogen

Samples	HNT content (wt %)	Temperature at 5% weight loss (°C)	Temperature at 10% weight loss (°C)	Temperature at maximum weight loss (°C)
PLA0	0	343.7	352.4	376.8
PLA1	1	341.5	350.3	377.8
PLA3	3	339.5	349.0	373.3
PLA5	5	339.6	347.0	370.0
PLA7	7	339.0	346.7	368.9

nanocomposites are lower than neat PLA with the addition of HNT. Compared with neat PLA, the value at 5% weight loss has a maximum decrease of 4.7°C with 7 wt % loading of HNT. The temperature at 10% weight loss and that at maximum weight loss rate show a similar trend as well. The previous investigations also showed the analogous thermal behavior in PLA/clay nanocomposites.[39,40] Ogata et al.[39] believed that the clay act as a decomposition accelerator at a higher temperature. But the specific reason for the decrease of thermal stability is still not clear. For the PLA/HNT nanocomposites used in this work, the decrease of thermal stability seems to likely result from the release of water vapor in HNT. As observed in the region between 50°C and 300°C in the TGA analysis of neat HNT (Figure 3), the release of some physically adsorbed water in the surface and the interlayer (weight loss of 0.9%) may, to some extent, contribute to accelerate the decomposition of the ester bond.[37]

Crystallization and Melting Behavior

DSC curves of the PLA with different HNT loading are shown in Figure 5. We can note that there is no crystalline peak occurs in the cooling process [Figure 5(a)], which is due to the rigid segments in its main chain. This indicates that the samples of neat PLA and PLA/HNT nanocomposites remain amorphous. Similar phenomena have been reported in previous articles.[41,42]

The glass transition temperature (T_g), cold crystallization temperature (T_c), melting temperature (T_m), cold crystallization heat of fusion (ΔH_c), and heat of fusion (ΔH_f) values for PLA/HNT nanocomposites corresponding to the DSC test [Figure 5(b)] are shown in Table II. It can be seen that the change in the heat flow observe to be around 64°C is attributed to the glass transition. We can also find that the T_g decreases slightly in PLA1 as compared with neat PLA. This behavior may be explained that the HNT reduces entanglements and interactions of PLA chain, causing a plasticization effect, promoting the motion of the polymer chains.[43,44] With the increase of HNT content, the T_g increases gradually, which indicates that the filler hinder the migration and diffusion of PLA molecular chains. Moreover, the shift peak in the cold crystallization of PLA/HNT nanocomposites is around 125°C which is about 10°C lower than neat PLA, implies that the nanocomposties are more easily crystallized. On the other hand, the heat of cold crystallization increases remarkably. These observations may indicate that the

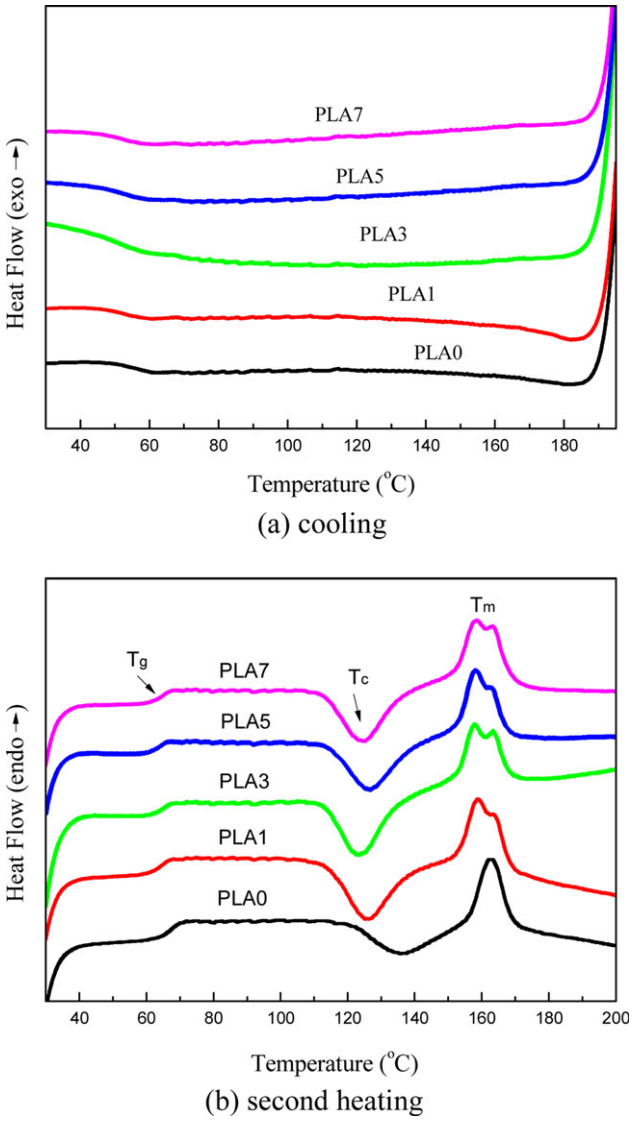

Figure 5. DSC curves of the PLA/HNT nanocomposites with different HNT contents: (a) cooling and (b) second heating. [Color figure can be viewed in the online issue, which is available at wileyonlinelibrary.com.]

presence of the HNT can act as nucleating agents on the crystallization of PLA.[45]

In the nanocomposites, the endothermic shoulder on melting appears at a relatively low temperature. Moreover, two distinct melting peaks are observed in Figure 5(b), in which could be linked to the formation of different crystal structures.[46–48] It has been reported that the double melting behavior of PLA is due to melt-reorganization.[49–51] The imperfect crystals formed in cold crystallization would reorganize into more orderly crystal structures.[52] Hoogsteen et al.[53] found that the helical conformations of the chain in the α and β-form had approximately the same energy. The ΔH_c of PLA/HNT nanocomposites are much higher when compared with neat PLA. Thus, the double melting behavior observed here is attributed to the addition of HNT. The effect of peak separation and formation of these two families of crystals with different T_m is more obvious with the content of 5 wt % nanotubes.

Table II. DSC Thermograms of Neat PLA and PLA/HNT Nanocomposites

Samples	HNT content (wt %)	T_g (°C)	T_c (°C)	ΔH_c (J/g)	T_m (°C)	ΔH_f (J/g)
PLA0	0	64.83	135.74	17.86	162.47	23.75
PLA1	1	63.09	125.32	27.77	158.90	26.02
PLA3	3	63.57	123.61	25.59	158.10	27.09
PLA5	5	64.85	126.88	25.47	157.97	27.45
PLA7	7	65.16	125.06	24.32	158.59	28.26

Mechanical Properties

The effect of HNT on the mechanical properties of PLA is depicted in Figure 6. It is seen that both the flexural modulus and tensile modulus of the material gradually increase with increase in HNT content. Comparing the neat PLA, the incorporation of HNT in the PLA matrix results in a significant enhancement in modulus (increase from 3380 MPa up to 4024 MPa in the flexural modulus, 1723 MPa up to 2047 MPa in tensile modulus, respectively). As demonstrated by SEM

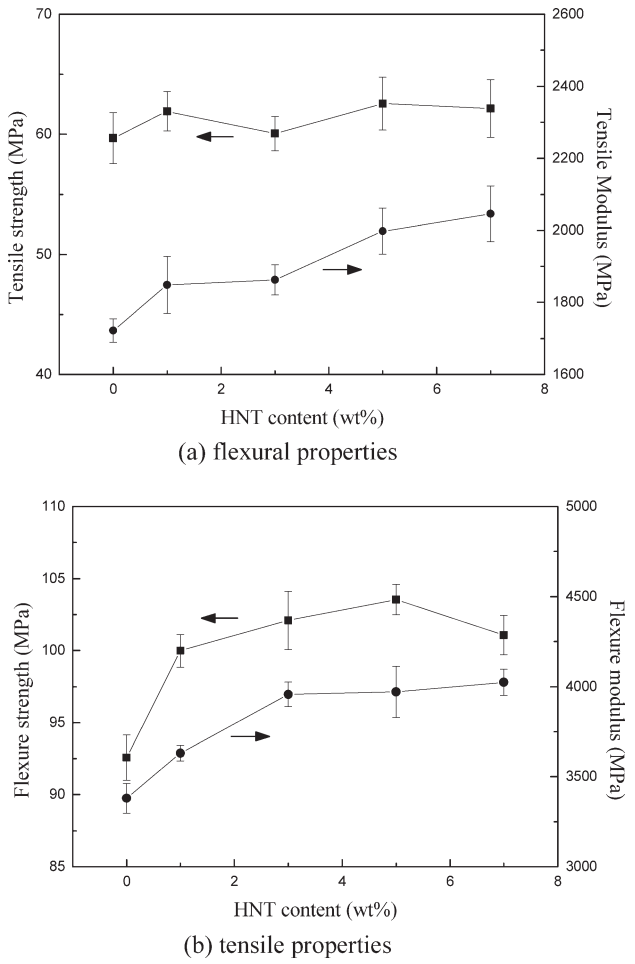

Figure 6. Effects of HNT content on mechanical properties of PLA/HNT nanocomposites (a) flexural properties and (b) tensile properties.

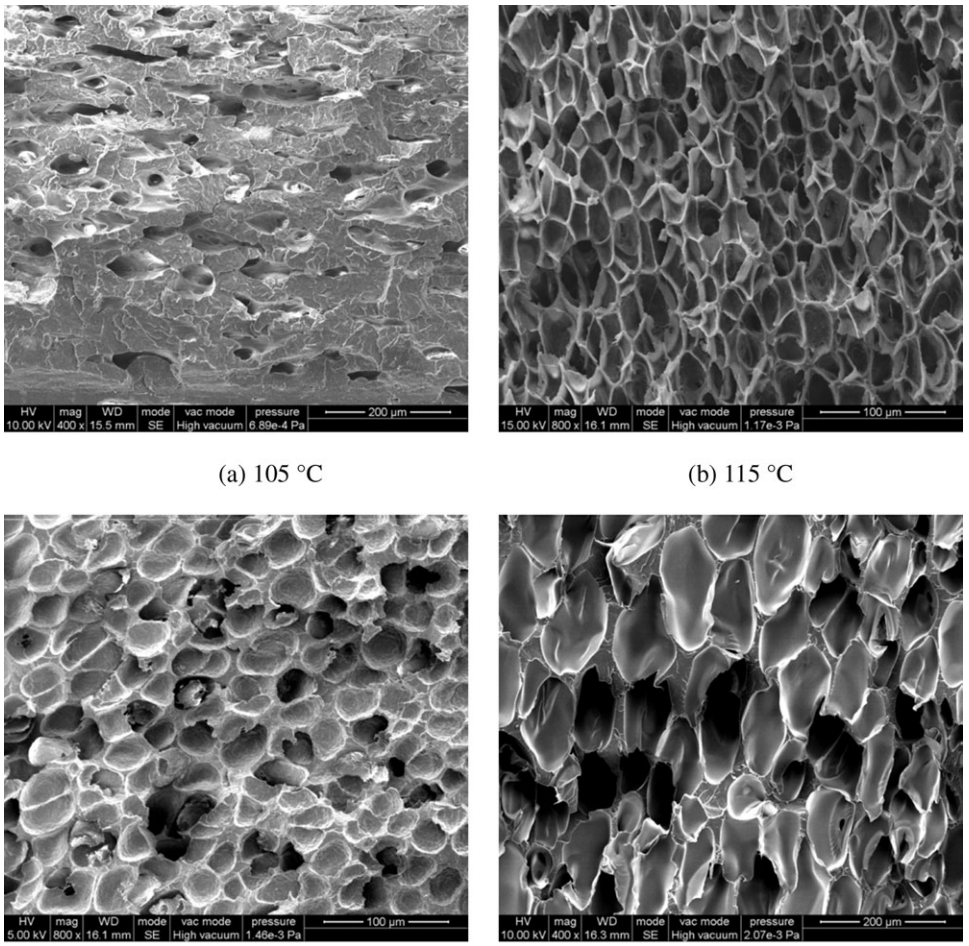

Figure 7. SEM micrographs of the cross sections of neat PLA foams at different foam temperature: (a) 105°C, (b) 115°C, (c) 125°C, and (d) 135°C.

micrographs in Figure 2, the HNT has a good dispersion in the PLA matrix. This increase in the modulus is attributed to the reinforcement introduced by the HNT that enhances the stiffness of the nanocompostie, allows a greater degree of stress transfer at the interface. The good dispersion of HNT in the matrix plays the main role in improving the mechanical properties of polymers at the low HNT loading which is also proposed by Guo et al.[54] and Guo and coworkers.[55] Figure 7(b) also shows that the PLA/HNT nanocomposites have no significant improvement in the tensile strength due to the poor interaction between the HNT and PLA matrix (as evidenced in the morphology study in Figure 2).

Foam Processing

The foaming process usually involves bubble nucleation, growth, and solidification. For batch microcellular foam processing,[56] the nucleation starts to occur within the polymer melt when the pressure is rapidly released and the bubble growth would be allowed a period of time. Consequently, the bubble would reach its critical size and solidified. It is well known that foam temperature is one of key factors influencing foam density and bubble size.[24,57] To find an optimum foaming temperature, the neat PLA without HNT was first foamed at the temperature of 105°C, 115°C, 125°C, and 135°C, respectively. Figure 7 shows the neat PLA foam structures of different foaming temperature for a given saturation pressure of 20 MPa. From the SEM micrograph in Figure 7(a), we can observe that the sample is lack of foam structure formation at the foaming temperature of 105°C. This is due to the melt elasticity of this polymer matrix is too strong to withstand the cell expansion. As we can see from Figure 7(b–d), the cell density decreases while the mean cell diameter and the cell-wall thickness show an increasing tendency with the foam temperature increasing. The results are due to a decrease in melt strength and melt viscosity of the polymer matrix.[58] A higher temperature will contribute to make the material softer and the cells easier to grow. Meanwhile, the cells will collapse and coalescence during the cell growth. As shown in Figure 7(d), the cells foamed at 135°C have a much higher cell diameter and lower cell density compare with the foams at 115°C [Figure 7(b)]. So, the sample foaming at the temperature of 115°C will have a better cell structure.

The effect of different contents of HNT from 1 to 7 wt % at fixed temperature and pressure on foam morphology is shown in Figure 8. From this figure, we can see that the nanocomposite foams show smaller cell size and larger cell density

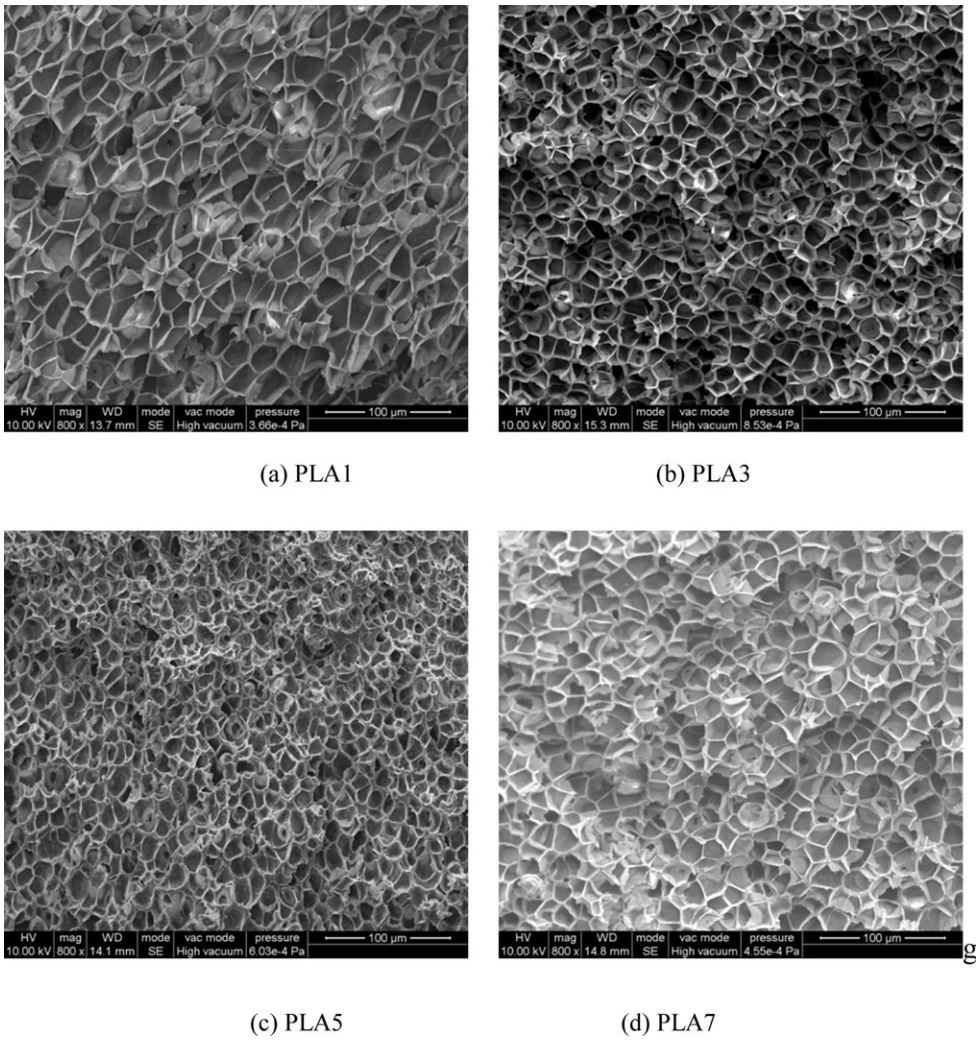

Figure 8. SEM micrographs of PLA/HNT nanocomposite foams with different content of HNT. The foaming condition was fixed at 20 MPa and 115°C.

compared with the neat PLA foams. As illustrated in Figure 9, the cell density increases sharply with the HNT content (from 7.38×10^8 cells/cm^3 for the neat PLA to 2.81×10^9 cells/cm^3 for the PLA5). Observations also suggest that the addition of HNT into PLA matrix could contribute to form open-cell structure of PLA/HNT nanocomposite foams. In addition, we also note that homogeneous cells are formed in the case of PLA/HNT nanocomposites in comparison with the nonuniform cell structure of neat PLA foam. These indicate that the HNT act as a nucleating agent for PLA/HNT nanocomposite foams.[21,24] More specifically, the cell nucleation took place at the boundary between the PLA matrix and the dispersed HNT. According to the classical nucleation theory,[59,60] the addition of nucleating agents can reduce the surface energy at the polymer-particle interface that promote heterogeneous nucleation. As demonstrated by Okamoto and coworkers,[24] the induction of dispersed nano-clay to PLA matrix could provide much more effective nucleation sites during foaming.

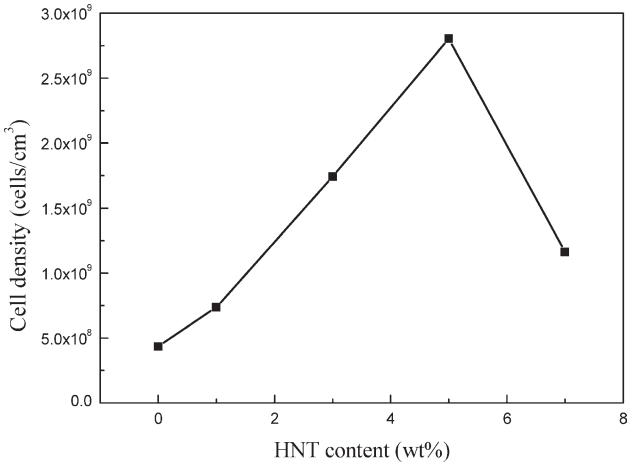

Figure 9. Cell density of neat PLA and PLA/HNT nanocomposites.

For the nanocomposite foams, the distribution function of cell size is calculated from SEM images and the results are presented in Figure 10. It can be observed that the cell size of the foams nicely obeys Gaussian distribution. Moreover, the width of the distribution, which corresponds to the distribution of the cell

Applied Polymer SCIENCE

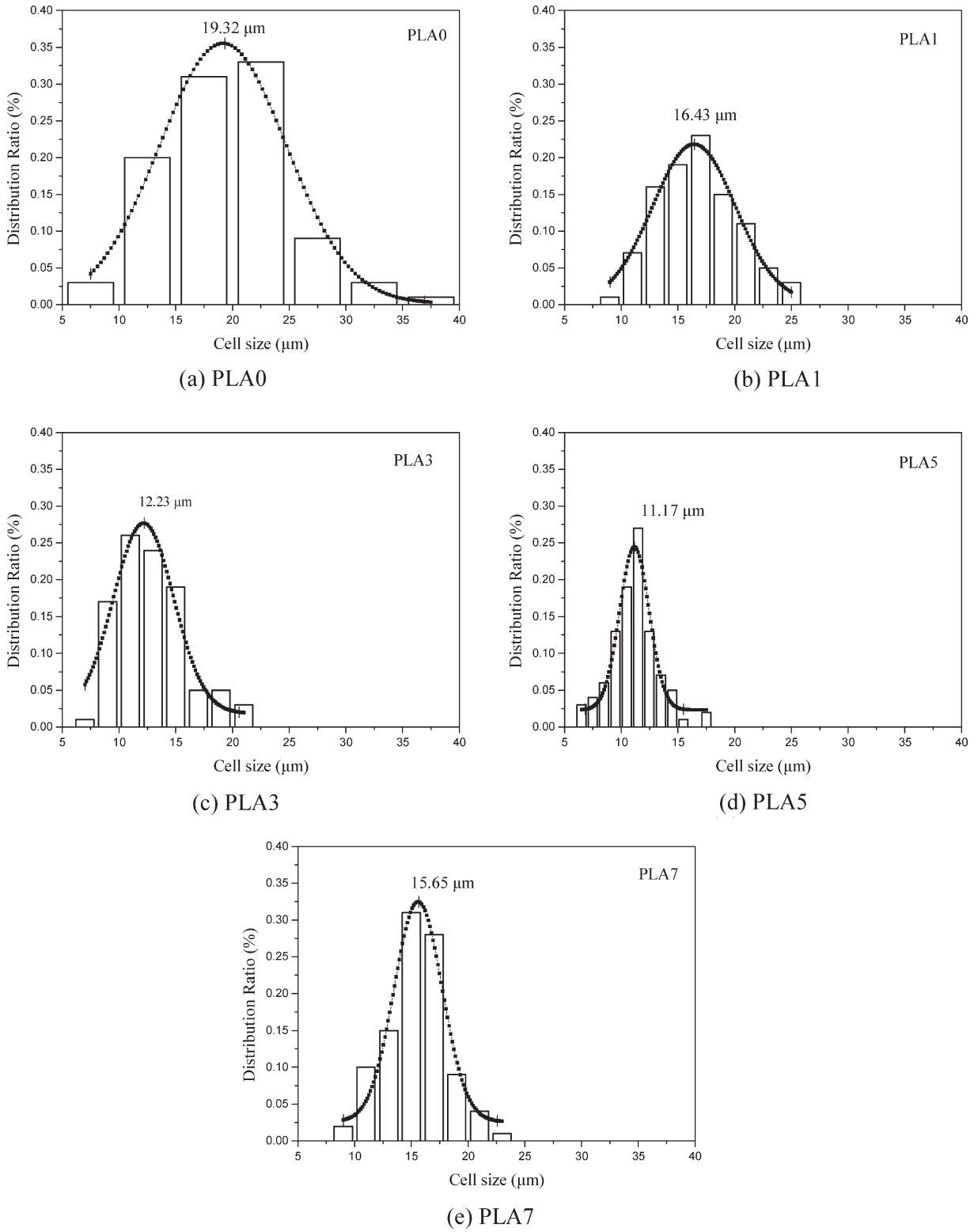

Figure 10. Cell-size distribution of PLA/HNT nanocomposite foams: (a) PLA0, (b) PLA1, (c) PLA3, (d) PLA5, and (e) PLA7.

size, becomes narrower with increasing HNT content. When the HNT content increases up to 5wt %, the PLA/HNT nanocomposite foam exhibits the narrowest cell size distribution, with cell size ranging between 6.3 and 17.7 μm. This is due to a great deal of well-dispersed HNT can improve the heterogeneous nucleation during the foaming process. With a further increase in the addition of the HNT, the cell size distribution broads to 8.8–23.7 μm. The cell density of PLA7 also decreases to

1.16×10^9 cells/cm^3 simultaneously. This phenomenon can be explained by the aggregation effect. Because of some HNT coalesced at a higher content, the bubbles around the coalesced HNT will have larger diameters during the bubble growth.

CONCLUSIONS

PLA/HNT nanocomposites were successfully achieved by melt compounding, and the HNT was first used for PLA foams. The morphology of the nanocomposite was characterized and the observation showed that HNT were well dispersed in the matrix but had a poor interfacial interaction with PLA. The thermal stability of the nanocomposite was reduced gradually with the increasing content of HNT. The DSC thermograms showed that the HNT could promote the cold crystallization of PLA due to the filler promoted the mobility of PLA molecular chain. Moreover, two distinct melting peaks were observed, suggesting that the formation of different crystal structures. Compared with neat PLA, the flexural properties of the nanocomposite were enhanced when the PLA was incorporated with HNT. The PLA/HNT nanocomposite foams were produced by batch foaming with Sc-CO_2. The addition of a small amount of HNT increased the cell density and reduced the mean cell size. The optimum HNT content for producing the PLA/HNT nanocomposite foams was determined to be 5 wt % with the highest cell density up to 2.81×10^9 cells/cm^3 and the narrowest cell size distribution between 6.3 and 17.7 μm.

ACKNOWLEDGMENTS

The authors are grateful to Imerys Tableware New Zealand Limited for halloysite nanotubes sample supply.

REFERENCES

1. Albertsson, A. C.; Varma, I. K. Degradable Aliphatic Polyesters; **2002**, *157*, 1.
2. Zhang, J. L.; Li, G.; Su, Y. Z.; Qi, R. R.; Ye, D. D.; Yu, J.; Huang, S. W. *J. Appl. Polym. Sci.* **2012**, *123*, 2996.
3. Zhang, H. L.; Liu, N. A.; Ran, X. H.; Han, C. Y.; Han, L. J.; Zhuang, Y. G.; Dong, L. S. *J. Appl. Polym. Sci.* **2012**, *125*, E550.
4. Gerard, T.; Budtova, T. *Eur. Polym. J.* **2012**, *48*, 1110.
5. Al-Itry, R.; Lamnawar, K.; Maazouz, A. *Polym. Degrad. Stab.* **2012**, *97*, 1898.
6. Zhang, Y.; Meng, B.; Chen, L.; Tao, J.; Wu, Z. H. *J. Appl. Polym. Sci.* **2012**, *125*, 952.
7. Ray, S. S.; Maiti, P.; Okamoto, M.; Yamada, K.; Ueda, K. *Macromolecules* **2002**, *35*, 3104.
8. Paul, M. A.; Alexandre, M.; Degee, P.; Henrist, C.; Rulmont, A.; Dubois, P. *Polymer* **2003**, *44*, 443.
9. Katiyar, V.; Gerds, N.; Koch, C. B.; Risbo, J.; Hansen, H. C. B.; Plackett, D. *J. Appl. Polym. Sci.* **2011**, *122*, 112.
10. Picard, E.; Espuche, E.; Fulchiron, R. *Appl. Clay Sci.* **2011**, *53*, 58.
11. Shibata, M.; Someya, Y.; Orihara, M.; Miyoshi, M. *J. Appl. Polym. Sci.* **2006**, *99*, 2594.
12. Balakrishnan, H.; Hassan, A.; Imran, M.; Wahit, M. U. *Polym.-Plast. Technol.* **2012**, *51*, 175.
13. Singh, S.; Ghosh, A. K.; Maiti, S. N.; Raha, S.; Gupta, R. K.; Bhattacharya, S. *Polym. Eng. Sci.* **2012**, *52*, 225.
14. Katiyar, V.; Gerds, N.; Koch, C. B.; Risbo, J.; Hansen, H. C. B.; Plackett, D. *Polym. Degrad. Stab.* **2010**, *95*, 2563.
15. Cao, H. L.; Wang, P.; Yuan, W. B.; Lei, H. F. *J. Appl. Polym. Sci.* **2010**, *115*, 1468.
16. Chiang, M. F.; Wu, T. M. *Compos. Sci. Technol.* **2010**, *70*, 110.
17. Shyang, C. W.; Kuen, L. S. *Polym. Polym. Compos.* **2008**, *16*, 263.
18. Jollands, M.; Gupta, R. K. *J. Appl. Polym. Sci.* **2010**, *118*, 1489.
19. Klempner, D.; Frisch, K. C. Handbook of Polymeric Foams and Foam Technology; Oxford University Press: New York, **1991**.
20. Fujimoto, Y.; Ray, S. S.; Okamoto, M.; Ogami, A.; Yamada, K.; Ueda, K. *Macromol. Rapid Commun.* **2003**, *24*, 457.
21. Di, Y. W.; Iannace, S.; Di Maio, E.; Nicolais, L. *J. Polym. Sci. Part B: Polym. Phys.* **2005**, *43*, 689.
22. Liao, X.; Nawaby, A. V.; Naguib, H. E. *J. Appl. Polym. Sci.* **2012**, *124*, 585.
23. Reignier, J.; Gendron, R.; Champagne, M. F. *Cell Polym.* **2007**, *26*, 83.
24. Ema, Y.; Ikeya, M.; Okamoto, M. *Polymer* **2006**, *47*, 5350.
25. Matuana, L. M.; Diaz, C. A. *Ind. Eng. Chem. Res.* **2010**, *49*, 2186.
26. Joussein, E.; Petit, S.; Churchman, J.; Theng, B.; Righi, D.; Delvaux, B. *Clay Miner.* **2005**, *40*, 383.
27. Du, M. L.; Guo, B. C.; Jia, D. M. *Eur. Polym. J.* **2006**, *42*, 1362.
28. Liu, M. X.; Guo, B. C.; Du, M. L.; Cai, X. J.; Jia, D. M. *Nanotechnology* **2007**, 18, 205709.
29. Ye, Y. P.; Chen, H. B.; Wu, J. S.; Chan, C. M. *Compos. Sci. Technol.* **2011**, *71*, 717.
30. Tang, Y. H.; Deng, S. Q.; Ye, L.; Yang, C.; Yuan, Q. A.; Zhang, J. N.; Zhao, C. B. *Compos. Part A: Appl. Sci. Manuf.* **2011**, *42*, 345.
31. Shamsi, M. H.; Luqman, M.; Basarir, F.; Kim, J. S.; Yoon, T. H.; Geckeler, K. E. *Polym. Int.* **2010**, *59*, 1492.
32. Liu, M. X.; Jia, Z. X.; Liu, F.; Jia, D. M.; Guo, B. C. *J. Colloid Interface Sci.* **2010**, *350*, 186.
33. Ning, N. Y.; Yin, Q. J.; Luo, F.; Zhang, Q.; Du, R.; Fu, Q. *Polymer* **2007**, *48*, 7374.
34. Jia, Z. X.; Luo, Y. F.; Guo, B. C.; Yang, B. T.; Du, M. L.; Jia, D. M. *Polym.-Plast. Technol.* **2009**, *48*, 607.
35. Han, X.; Shen, J.; Huang, H.; Tomasko, D. L.; Lee, L. J. *Polym. Eng. Sci.* **2007**, *47*, 103.
36. Prashantha, K.; Schmitt, H.; Lacrampe, M. F.; Krawczak, P. *Compos. Sci. Technol.* **2011**, *71*, 1859.
37. Carli, L. N.; Crespo, J. S.; Mauler, R. S. *Compos. Part A: Appl. Sci. Manuf.* **2011**, *42*, 1601.

38. Gilman, J. W. *Appl. Clay Sci.* **1999**, *15*, 31.
39. Ogata, N.; Jimenez, G.; Kawai, H.; Ogihara, T. *J. Polym. Sci. Part B: Polym. Phys.* **1997**, *35*, 389.
40. Wu, D.; Wu, L.; Wu, L.; Zhang, M. *Polym. Degrad. Stab.* **2006**, *91*, 3149.
41. Pluta, M.; Galeski, A.; Alexandre, M.; Paul, M. A.; Dubois, P. *J. Appl. Polym. Sci.* **2002**, *86*, 1497.
42. Souza, D. H. S.; Borges, S. V.; Dias, M. L.; Andrade, C. T. *Polym. Compos.* **2012**, *33*, 555.
43. Lecouvet, B.; Gutierrez, J. G.; Sclavons, M.; Bailly, C. *Polym. Degrad. Stab.* **2011**, *96*, 226.
44. Du, M. L.; Guo, B. C.; Cai, X. J.; Jia, Z. X.; Liu, M. X.; Jia, D. M. *e-Polymers* **2008**, *130*, 1.
45. Touny, A. H.; Lawrence, J. G.; Jones, A. D.; Bhaduri, S. B. *J. Mater. Res.* **2010**, *25*, 857.
46. Yasuniwa, M.; Sakamo, K.; Ono, Y.; Kawahara, W. *Polymer* **2008**, *49*, 1943.
47. Kawai, T.; Rahman, N.; Matsuba, G.; Nishida, K.; Kanaya, T.; Nakano, M.; Okamoto, H.; Kawada, J.; Usuki, A.; Honma, N.; Nakajima, K.; Matsuda, M. *Macromolecules* **2007**, *40*, 9463.
48. Yasuniwa, M.; Tsubakihara, S.; Sugimoto, Y.; Nakafuku, C. *J. Polym. Sci. Part B: Polym. Phys.* **2004**, *42*, 25.
49. Di Lorenzo, M. L. *J. Appl. Polym. Sci.* **2006**, *100*, 3145.
50. Ling, X.; Spruiell, J. E. *J. Polym. Sci. Part B: Polym. Phys.* **2006**, *44*, 3378.
51. Shieh, Y.-T.; Liu, G.-L. *J. Polym. Sci. Part B: Polym. Phys.* **2007**, *45*, 1870.
52. Vink, E. T. H.; Rabago, K. R.; Glassner, D. A.; Gruber, P. R. *Polym. Degrad. Stab.* **2003**, *80*, 403.
53. Hoogsteen, W.; Postema, A. R.; Pennings, A. J.; Brinke, G.; Zugenmaier, P. *Macromolecules* **1990**, *23*, 634.
54. Guo, B. C.; Zou, Q. L.; Lei, Y. D.; Jia, D. M. *Polym. J.* **2009**, *41*, 835.
55. Liu, C.; Luo, Y. F.; Jia, Z. X.; Zhong, B. C.; Li, S. Q.; Guo, B. C.; Jia, D. M. *Express Polym. Lett.* **2011**, *5*, 591.
56. Han, X. M.; Koelling, K. W.; Tomasko, D. L.; Lee, L. J. *Polym. Eng. Sci.* **2003**, *43*, 1206.
57. Kang, D. J.; Xu, D.; Zhang, Z. X.; Pal, K.; Bang, D. S.; Kim, J. K. *Macromol. Mater. Eng.* **2009**, *294*, 620.
58. Arora, K. A.; Lesser, A. J.; McCarthy, T. J. *Macromolecules* **1998**, *31*, 4614.
59. Colton, J. S.; Suh, N. P. *Polym. Eng. Sci.* **1987**, *27*, 493.
60. Colton, J. S.; Suh, N. P. *Polym. Eng. Sci.* **1987**, *27*, 485.